Altered hippocampal astroglial metabolism is associated with aging and preserved spatial learning and memory

Jeremy Ebersole[a], Gregory Rose[a,b,c], Tore Eid[d], Kevin Behar[e,f], Peter Patrylo[a,b,c,*]

[a] Department of Physiology, Southern Illinois University School of Medicine, Carbondale, IL, USA
[b] Department of Anatomy, Southern Illinois University School of Medicine, Carbondale, IL, USA
[c] Center for Integrated Research in the Cognitive and Neural Sciences, Southern Illinois University School of Medicine, Carbondale, IL, USA
[d] Department of Laboratory Medicine, Yale University School of Medicine, New Haven, CT, USA
[e] Department of Psychiatry, Yale University School of Medicine, New Haven, CT, USA
[f] MRRC Neurometabolism Research Laboratory, Yale University School of Medicine, New Haven, CT, USA

ARTICLE INFO

ABSTRACT

An age-related decrease in hippocampal metabolism correlates with cognitive decline. Hippocampus-dependent learning and memory requires glutamatergic neurotransmission supported by glutamate-glutamine (GLU-GLN) cycling between neurons and astrocytes. We examined whether GLU-GLN cycling in hippocampal subregions (dentate gyrus and CA1) in Fischer 344 rats was altered with age and cognitive status. Hippocampal slices from young adult, aged cognitively-unimpaired (AU) and aged cognitively-impaired (AI) rats were incubated in artificial cerebrospinal fluid (aCSF) containing 1-^{13}C-glucose to assess neural metabolism. Incorporation of ^{13}C-glucose into glutamate and glutamine, measured by mass spectroscopy/liquid chromatography tandem mass spectroscopy, did not significantly differ between groups. However, when ^{13}C-acetate, a preferential astrocytic metabolite, was used, a significant increase in ^{13}C-labeled glutamate was observed in slices from AU rats. Taken together, the data suggest that resting state neural metabolism and GLU-GLN cycling may be preserved during aging when sufficient extracellular glucose is available, but that enhanced astroglial metabolism can occur under resting state conditions. This may be an aging-related compensatory change to maintain hippocampus-dependent cognitive function.

1. Introduction

A consequence of lengthening human life span has been an increased occurrence of age-related neurological impairments, including mild-cognitive impairment (MCI) and dementias (www.Alz.org). Numerous factors can contribute to aging-related cognitive decline, including altered ion channels/receptors (Disterhoft et al., 1996; Thibault and Landfield, 1996; Pereda et al., 2019; Kumar and Foster, 2019), compromised

synaptic plasticity (Landfield and Lynch, 1977; Tombaugh et al., 2002; Rosenzweig and Barnes, 2003), mitochondrial dysfunction (Liu et al., 2002; Navarro et al., 2008), calcium dysregulation (Toescu and Verkhratsky, 2007; Oh et al., 2013), altered network connectivity (Patrylo and Williamson 2007; Tardif et al., 2018), increased neuroinflammation (d'Avila et al., 2018; Navakkode and Soong, 2018), and increased oxidative stress (Droge and Schipper et al., 2007; Ghosh et al., 2012). In Alzheimer's (AD) or other neurological diseases, the overproduction of β-amyloid oligomers and plaques, as well as hyper-phosphorylated tau and neurofibrillary tangles, may play a role as well (Crimins et al., 2013; Raskin et al., 2015; Morley and Farr, 2014; Tu and Xu 2014).

It has also been suggested that declining brain metabolism is likely to be a constraint for healthy cognitive aging, and that targeting brain hypometabolism in conjunction with other therapeutic strategies may be key to successfully limit cognitive decline during aging (Motsinger-Reif et al., 2013; Daulatzai 2017; Croteau et al., 2018). Reductions in glucose utilization in the hippocampus, a brain structure that is a critical mediator of explicit learning and

memory, occur during both normal and pathological aging (e.g., AD), with the degree of hypometabolism being correlated with the extent of cognitive decline. For example: 1) modern imaging techniques (PET and MRS) have revealed that decreased brain energy metabolism, specifically related to glucose, is associated with aging, MCI and Alzheimer's disease (Mosconi et al., 2008; Croteau et al., 2018; Roy et al., 2014; Riederer et al., 2018); 2) aged rats with impaired performance on the Morris water maze, a hippocampus-dependent task, exhibit lower levels of hippocampal 2-deoxyglucose (2-DG) uptake compared to young and aged rats with intact hippocampal function (Gage et al, 1984); and 3) the hippocampus of aged versus adult rats exhibits a relative reduction in extracellular glucose concentration during training on a spontaneous alternation task (McNay and Gold, 2001). Since glucose is the primary energy substrate of the adult mammalian brain, these findings suggest that a decline in hippocampal metabolic function very likely contributes to age-related memory deficits.

Aging-related hippocampal hypometabolism can impair glutamatergic neurotransmission due to altered neural metabolism and glutamate-glutamine cycling (GLU-GLN) between neurons and astrocytes. Several studies suggest that GLU-GLN cycling may be decreased in humans and animal models during aging and Alzheimer's disease (Boumezbeur et al., 2010; Nilsen et al., 2012; Riese et al., 2015; Huang et al., 2017, but see Fayed et al., 2014; Manyevitch et al., 2018). While neurons are directly involved with information processing in the hippocampus, astroglia are also key players due to their role in regulating glutamatergic and GABAergic neurotransmission. Astrocytes take up synaptically released glutamate to effectively terminate the neuronal signaling of the transmitter (Rothstein et al., 1996). The astrocytes then either oxidize the glutamate or convert it to glutamine via glutamine synthetase (Martinez-Hernandez et al., 1977; Hertz et al., 2007). This glutamine is shuttled back to glutamatergic neurons, possibly via a sodium coupled neutral amino acid transporter (Chaudhry et al., 2002; Jenstad et al., 2009) and converted to glutamate via phosphate activated glutaminase (Kvamme et al., 2001). This GLU-GLN cycle helps replenish presynaptic glutamate stores and is a dynamic process that is directly coupled to neuroenergetics (Lennie 2003; Rothman et al., 1999, 2003, 2011; Escartin et al., 2006).

Therefore, age-related changes in astrocytic metabolism could result in alterations in GLU-GLN cycling and cognitive function. However, few studies of astroglial metabolism during aging have been published (Boumezbeur et al., 2010). The goal of the present experiments was to assess whether age-related changes in hippocampal neuronal or astrocytic metabolism occur and whether the changes are related to cognitive performance. Young adult (YA) and aged Fischer 344 rats were behaviorally evaluated using the Morris water maze task to classify the aged rats as cognitively unimpaired (AU) or impaired (AI) based on statistical criteria (Tombaugh et al., 2002; Rowe et al., 2007). Hippocampal slices were then prepared from these animals and in vitro metabolic studies were performed under non-stimulated conditions (resting state). We initially hypothesized that age-related cognitive impairment would be associated with declines in neuron and astrocyte metabolism. However, instead we found that increased astrocytic metabolism (reflected as enhanced conversion of acetate to glutamate) was observed under resting state conditions in slices from aged rats with preserved water maze performance.

2. Materials and methods

2.1. Animals

Male Fischer-344 rats (young adults 3-7 months of age; aged rats $\geq$ 24 months of age) were obtained either from the National Institutes of Health colony at Harlan laboratories (Indianapolis, IN) or from Hilltop Laboratories (Scottdale, PA). Animals were then pair-housed in the Southern Illinois University Carbondale vivarium on a 12hr/12hr light dark cycle and were provided food and water ad libitum. All experiments were approved by the Southern Illinois University Carbondale Institutional Animal Care and Use Committee and comply with the guidelines set forth by the National Institutes of Health. All animals were behaviorally tested as described below. The numbers of animals used to evaluate hippocampal GLU/GLN cycling are detailed in Table 1.

2.2. Behavioral testing

The rats were behaviorally evaluated using the Morris water maze task. The water maze consisted of a circular tank (1.5 meters in diameter) located in the center of an isolated room and surrounded by salient visual cues. A video camera was mounted overhead to provide real-time monitoring and record swimming behavior (Polytrack, San Diego Instruments, San Diego, CA). Hidden platform training consisted of fifteen trials over five days (3 trials/day) with a clear Plexiglas escape platform (12 cm diameter) submerged 1 cm below the surface of the water (20-23 °C) in the center of one of the quadrants. Trial durations were a maximum of 90 seconds; rats that failed to find the platform by 90 seconds were hand guided to it. The rats remained on the platform for 30 seconds, after which they were dried with a towel and returned to their home cage for an intertrial interval of 20-30 minutes. Starting positions were located around the rim of the pool in the center of the three quadrants that did not contain the platform and were pseudo-randomly alternated. A probe test (30 seconds) was subsequently performed following hidden platform training. For the probe test, the platform was lowered out of reach of the rats. The number of platform location crosses, mean distance from the platform location, and total swim distance were recorded.

On the sixth day, rats were given three visible platform trials to assess for visual or motor deficits or a lack of motivation. During these trials, the platform was elevated above the water and moved to a novel location for each trial. Rats need to swim to the visible platform with an average of less than 40 seconds for the three trials to be included in the metabolic study. None of the rats tested failed to meet this criterion. However, one AU rat and 3 AI rats were excluded because it was determined at sacrifice that they had pituitary tumors. One other AU rat died before the visible platform trials were run. None of the behavioral data from these rats was included in the analysis, and their hippocampi were not used for metabolic studies.

Swim times and distances to find the hidden platform were recorded for all training trials. To classify aged rats as unimpaired or impaired, the average swim distance of each animal over training days 3-5 was compared to the average of the young adult (YA) rats. Using methodology from our previous work (Tombaugh et al., 2002), aged rats with an average swim distance < 0.5 standard deviation from YA rats were classified as aged-unimpaired (AU), while aged rats with swim distance averages $\geq$ 3 standard deviations were considered age-impaired (AI).

Table 1
Behaviorally tested rats used to generate hippocampal tissues to evaluate GLU/GLN cycling.

Group	Total	Neuronal (^{13}C-glucose) only	Astrocytic (13C-acetate) only	Used for both
YA	14	1	3	10
AU	10	3	0	7
AI	9	1	2	6

2.3. Hippocampal slice preparation

Rats were terminally anesthetized with sodium pentobarbital (100 mg/kg; i.p.) and their brains were rapidly removed and placed in chilled artificial cerebral spinal fluid (aCSF, 1-2°C) equilibrated with 95% O_2 / 5% CO_2 for one minute. The aCSF was composed of (in mM concentrations): 124 NaCl, 3 KCl, 2 $CaCl_2$, 26 $NaHCO_3$, 1.3 $MgSO_4$, 1.25 NaH_2PO_4, and 10 glucose (pH 7.2 - 7.4; 290-300 mOsmols). Subsequently, brains were bisected mid-sagittally and the dorsal surface was secured to a cutting platform. Transverse slices (400 μm thick) were cut from the middle one-third of the hippocampus using a Vibratome (Ted Pella Instruments, Redding, CA).

2.4. Slice incubation with ^{13}C labeled glucose, or acetate

Slices were randomly selected and placed into wells of a 24-well tissue culture plate (one slice per well) containing 800 μL aCSF. The tissue culture plate was placed into an incubation chamber that was maintained at 34 - 35°C and continuously exposed to humidified 95% O_2 / 5% CO_2 gas. Slices were equilibrated for two hours and then transferred into wells containing aCSF with the appropriate ^{13}C-labeled compound (10 mM 1-^{13}C-glucose or 1 mM 2-^{13}C-acetate in aCSF with 10 mM non-labeled glucose). After a 2-6-hour incubation period (see below; Results) slices were rinsed with cold aCSF (1-2°C) to halt metabolism and the dentate gyrus (which included the hilus) and CA1 were cut from the slices under a dissecting microscope. A schematic illustration of the subregion dissection borders is shown in Supplementary Fig. S1. Tissue from each region and condition was subsequently collected, frozen on dry ice, and stored at -80°C until chemical analysis.

2.5. Quantification of ^{13}C labeled amino acids and calculation of percent labeling

The methods for determining ^{13}C labeling of glutamate and glutamine in isolated hippocampal subregions were adapted from the protocol described by Waagepetersen et al (2000). Specifically, the proteins were precipitated from thawed samples by adding liquid chromatography/mass spectrometry (LC/MS) grade methanol followed by microbead homogenization (FastPrep tissue homogenizer, MP Biomedicals, Solon, OH). The samples were then centrifuged (14,000 g, 5 minutes, 4°C) and the supernatant transferred to separate vials kept on ice. Calibration standards, quality control samples, and tissue supernatants were then derivatized and extracted using a modified version of a supplied protocol (LC/MS EZ-fast Free Amino Acid Kit - Physiological, Phenomenex, Torrance, CA). Modifications made to the protocol entailed: 1) reducing the amount of sample to 6 μL; 2) diluting the internal standard solution 1:10 with water and spiking with U-^{13}C-glutamate (1 μmol/L) and U-^{13}C-glutamine (5 μmol/L); 3) adding 194 μL of the spiked internal standard solution to each sample for system auto-correction of response fluctuations or sample loss though the chromatography step; and 4) evaporating the samples to dryness using nitrogen gas at ambient temperature and then storing (< four weeks) in capped autosampler glass vials at -80 °C until LC/MS analysis.

On the day of analysis, samples were reconstituted with 50 μL of 50% methanol/H_2O and transferred to low volume autosampler vials with pre-slit PTFE/silicone septum caps (Waters Corporation, Milford, MA). Individual samples were separated by ultraperformance liquid chromatography using an Acquity UPLC HSS T3, 1.8 μm 2.1 × 100 mm column with a Waters Acquity Separation Module (Waters Corporation, Milford, MA). Mobile phases were 2 mM ammonium acetate to 0.1% formic acid in water and 2 mM ammonium acetate to 0.1% formic acid in methanol. Amino acids were then separated by gradient elution. Glutamate and glutamine were quantified from the column effluent using an electrospray interface into a triple quadrupole tandem mass spectrometer in positive ion mode (Waters/Micromass Quattro Micro API, Waters Corporation, Milford, MA). The mass-to-charge (m/z) transitions used to quantify unlabeled, singly-labeled (M1), and doubly labeled (M2) glutamate were 318>172 m/z, 319>173 m/z, and 320>174 m/z, respectively. For glutamine the transitions were 275>172 m/z, 276>73 m/z, and 277>174 m/z, respectively. Triple ^{13}C-labels were not examined as they are not significantly represented in the total isotope composition (< 0.1%). The limit of quantitation (defined as a signal-to-noise ratio of ≥ 10) was 100 nM for glutamate and 500 nM for glutamine. Accuracy (defined as recovery from an accurately weighed-in calibrator solution) was >90%, and between-run precision of relevant isotope ratios was ≤ 10% (coefficient of variation). The concentrations of unlabeled, single- and double-labeled amino acids were calculated using MassLynx software, which compares the tissue concentrations to a standard curve using commercial amino acid standards.

2.6. Calculation of glutamate and glutamine labeling

The percent ^{13}C labeling of glutamate and glutamine were calculated using the peak area for each isotope. The general formula used was [% labeled = (labeled amino acid / total amino acid) * 100] and was adapted from the protocol used by Dericioglu et al. (2008). The calculation of percent labeling was as follows:

Total labeling (%) = [(amino acid containing one ^{13}C + amino acid containing two ^{13}Cs) / (unlabeled amino acid + amino acid containing one ^{13}C + amino acid containing two ^{13}Cs)] * 100

Single labeling (M1; %) = [amino acid containing one ^{13}C / (unlabeled amino acid + amino acid containing one ^{13}C + amino acid containing two ^{13}Cs)] * 100

Double labeling (M2; %) = [amino acid containing two ^{13}Cs / (unlabeled amino acid + amino acid containing one ^{13}C + amino acid containing two ^{13}Cs)] * 100

Note that this approach includes the natural ^{13}C abundance which is constant throughout all samples and therefore will not contribute to any differences in labeling due to the experimental paradigm.

2.7. Statistics

Statistical analysis was performed using GraphPad Prism, version 7.02 (GraphPad Software, San Diego, CA). Morris water maze performance measures were compared between groups (YA, AU, and AI) over all training days using a repeated measure ANOVA

with Bonferroni post hoc tests to assess individual days. Additionally, simple one-way and two-way ANOVAs with Bonferroni post hoc tests were used for between-group comparisons of labeling measures. When significant differences in variance were present the nonparametric Kruskal-Wallis test was applied, with the Dunn's Multiple Comparisons Test for post hoc analysis. Data used for analysis was based the mean value of each animal; in the metabolic studies, this was derived from 3-4 hippocampal slices per rat.

3. Results

3.1. Time course of glutamate and glutamine labeling with ^{13}C-labeled compounds

Since most previous 1-^{13}C-glucose and 2-^{13}C-acetate incorporation studies were done in vivo, a time course study was first performed for both compounds using hippocampal slices prepared from non-behaviorally characterized YA Fischer 344 rats (3-4 months old, n = 4). Hippocampal slices were prepared and incubated in either 10 mM 1-^{13}C-glucose aCSF, or 10 mM glucose aCSF supplemented with 1 mM 2-^{13}C-acetate, for 2, 4, or 6 hrs. Subsequently, ^{13}C-labeling of glutamate and glutamine was quantified in the dentate gyrus and CA1 using LC/MS. The total, single (M1) and double (M2) percent labeling of glutamate and glutamine were assessed and compared. Prior in vivo studies suggest that when ^{13}C labeled glucose is used it results in an initial labeling of glutamate mainly in neurons, with subsequent transfer of the glutamate to astrocytes and conversion to glutamine. However, some glutamine labeling is also likely to occur directly in astrocytes from the labeled glucose. In contrast, when ^{13}C labeled acetate is used, glutamine labeling is primarily due to acetate metabolism preferentially occurring in astrocytes, with the labeling of glutamate subsequently reflecting the conversion of labeled glutamine into glutamate in neurons (Serres et al, 2008; Deelchand et al, 2009; Patel et al, 2010; Wyss et al, 2011).

The time course data for 1-^{13}C-glucose incorporation is shown in Supplementary Fig. S2. In both the dentate gyrus and hippocampal area CA1, total, single and double ^{13}C labeled glutamate levels were greater than that of glutamine. The labeled glutamate levels (total, M1 and M2) exhibited an exponential increase during the entire incubation period, while ^{13}C labeled glutamine increased from two to four hours in both regions but did not further increase at six hours. Data for the time course of 2-^{13}C-acetate incorporation is shown in Supplementary Fig. S3. In both the dentate gyrus and CA1, total, single- and double-labeled glutamine levels were greater than that of ^{13}C labeled glutamate at the 2- and 4-hour time points, consistent with acetate being a preferential astrocytic substrate. Indeed, enrichment of ^{13}C glutamine appeared to reach asymptotic levels at the two-hour time point in both the dentate gyrus and CA1 in vitro, with no real change in labeling observed at the later time points. In contrast, the percent of total, single and double ^{13}C labeled glutamate increased in both brain regions over the entire time period. The asymptotic increase in single-labeled glutamine observed, coupled with the continued increase of single-labeled glutamate, is consistent with the C4 labeling pattern reported in vivo (Moreno et al., 2001; Rothman et al., 2003) and suggests that labeled glutamine was being transferred to neurons. Since the labeling of glutamine appeared to be asymptotic at two hours, this time point was chosen for subsequent studies to provide a measure of glutamine transfer when astroglial metabolism had reached steady-state conditions.

3.2. Water maze performance in YA, AU and AI Fischer 344 rats

Aged rats were classified as aged-unimpaired (AU) or aged-impaired (AI) by comparing their individual averaged swim distances over the last three days of hidden platform training relative to that of the young adult rats (YA). The water maze performance of these groups is shown in Fig. 1.

Overall, swim distance significantly decreased over the five days of hidden platform training in all groups ($F_{4,150}$ = 30.65, p < 0.0001). Additionally, there was a significant effect of group ($F_{2,150}$ = 29.01, p < 0.0001), as well as an interaction between the day of training and group ($F_{8,150}$ = 3.74, p < 0.001). Post hoc testing demonstrated that AI rats had significantly greater swim distances on training days 3-5 compared to the YA and AU rats ($p \leq$ 0.001; Fig. 3A). No differences were noted in performance on any training day in YA versus AU rats. Average swim speeds (cm/sec) over the five-day training period were: YA – 31.5 ± 1.4; AU – 28.9 ± 1.4; AI – 25.5 ± 1.1. Overall, there was a significant difference between groups ($F_{2,31}$ = 4.60, p < 0.018). Post hoc testing indicated that this was due to difference between YA and AI rats (p = 0.015). No difference in swim speed was found when AU and AI rats were compared (p = 0.33).

To assess memory retention, a probe test was performed following the last training trial on day five. As shown in Fig. 3B, while YA and AU animals exhibited comparable numbers of platform crosses and mean swim distances from the platform position, AI rats exhibited a significant decrease in the number of platform crosses ($p \leq$ 0.01 vs. AU; p < 0.0001 versus YA) and an increase in mean swim distance from the platform (p < 0.0001 vs. YA and AU), indicating that memory was compromised in the AI rats. YA rats swam somewhat further than the other two groups during the probe trial (YA: 1237 ± 28 cm; AU: 1074 ± 28 cm; AI: 1046 ± 53 cm; p < 0.01 for YA vs. either group), but for this measure AU and AI rats were not different from each other. No differences between groups were observed for the visible platform trials (Table 2).

3.3. Stable isotope tracing of metabolism relative to aging and cognitive status

A total of 11 YA (5-7 months), 10 AU (24-27 months), and 7 AI rats (24-27 months) were used for the ^{13}C-labeled glucose experiments. Hippocampal slices prepared from these behaviorally classified rats were exposed to aCSF containing 10 mM of 1-^{13}C-glucose for two hours with labeled glutamate and glutamine quantified by LC/MS/MS. Because glutamate is concentrated in neurons, while glutamine is thought to be largely produced and contained in astrocytes (Badar-Goffer et al, 1990), the labeling of each of these amino acids was considered separately.

When total labeling was compared between the hippocampal subregions (DG vs. CA1) after incubation with ^{13}C- glucose, significantly greater levels of ^{13}C-labeled glutamate were observed in the dentate gyrus vs. CA1 in all three groups (Fig. 2 top, p < 0.0001 for YA and AU, p < 0.01 for AI), suggesting that the dentate gyrus may exhibit greater metabolic activity. In contrast, no inter-regional differences were noted in total ^{13}C labeled glutamine (Fig. 2 top). When the total percent enrichment of ^{13}C labeled glutamate and glutamine was compared between groups (YA versus AU versus AI) no differences were observed for product in either the dentate gyrus [glutamate ($F_{2,25}$ = 2.18; p = 0.14) or glutamine ($F_{2,25}$ = 0.86; p = 0.44)] or CA1 [glutamate ($F_{2,25}$ = 1.49; p = 0.24) or glutamine ($F_{2,25}$ = 0.37; p = 0.70)] (Fig. 3). Further, analysis of the percentage of single- and double- labeled ^{13}C glutamate and glutamine also did not reveal any significant differences between YA, AU and AI rats (Fig. 3). These findings suggest that while there are inter-regional differences in glucose utilization in resting hip-
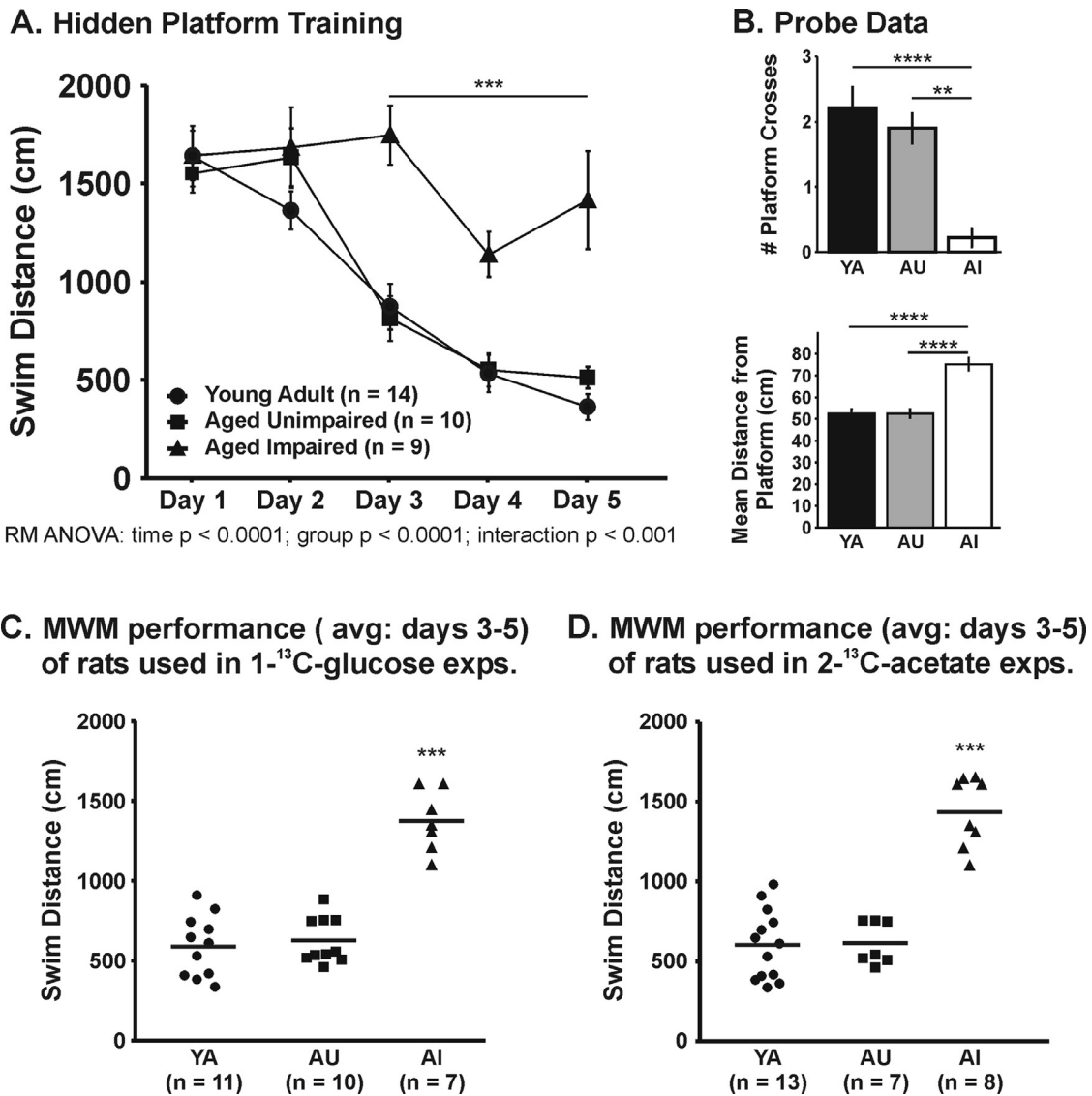
A. Hidden Platform Training

RM ANOVA: time p < 0.0001; group p < 0.0001; interaction p < 0.001

B. Probe Data

C. MWM performance (avg: days 3-5) of rats used in 1-^{13}C-glucose exps.

D. MWM performance (avg: days 3-5) of rats used in 2-^{13}C-acetate exps.

Fig. 1. Morris water maze (MWM) data from young adult (YA), aged cognitively-unimpaired (AU), and aged cognitively impaired (AI) rats. (A) Swim distance to find the hidden platform over the 5-day training period. Note the significant difference in swim distance on days 3-5 between the AI versus YA and AU rats ($^{***}p \leq 0.001$). (B) Probe data revealed a significant decrease in the number of platform location crosses and the mean swim distance from the location of the platform by AI versus AU and YA rats (number of crosses $^{**}p \leq 0.01$; $^{****}p \leq 0.0001$; mean swim distance $^{****}p \leq 0.0001$), suggesting that memory was impaired in the AI group. (C and D) The average MWM performance on days 3-5 of the individual YA, AU and AI rats that were subsequently used for the 1-^{13}C-glucose and 2-^{13}C-acetate cycling experiments, respectively; (AI compared to YA and AU; post-hoc analysis $^{***} p \leq 0.001$).

Table 2
Performance in the visible platform test.

Group	Swim time (sec, mean ± sem; range)	Distance (cm, mean ± sem; range)
Adult	6.5 ± 0.9; range 3.0–13.4	207 ± 28 cm; range 112–385 cm
AU	8.6 ± 1.3; range 2.9–15.0	241 ± 40 cm; range 107–429 cm
AI	10.3 ± 1.0; range 6.5–16.1	263 ± 26 cm; range 152–418 cm

No significant differences were found between any of the groups.

pocampal slices of rats (DG > CA1), the overall utilization of glucose and GLU-GLN cycling does not appeared altered with aging or cognitive status.

Experiments were performed using 2-^{13}C-acetate to preferentially examine the contribution of astrocytes to neural metabolism and GLU-GLN cycling under resting state conditions relative to age and cognitive status. Hippocampal slices obtained from a total of 13 YA, 7 AU and 8 AI rats were exposed to aCSF containing 10 mM un-labeled glucose plus 1 mM 2-^{13}C-acetate for two hours.

Compared to the data obtained using ^{13}C glucose, adding 1 mM 2-^{13}C-acetate to the aCSF resulted in a greater percent enrichment of total glutamine labeling relative to total percent glutamate labeling in both the dentate gyrus and CA1 of all three groups (Fig. 2 bottom and Fig. 4). This likely reflects the preferential metabolism of acetate in astrocytes leading to a preferential labeling of glutamine (i.e., precursor), which is subsequently transferred to neurons and converted to labeled glutamate (i.e., product). Overall, the enrichment of total labeled glutamine and glutamate was significantly
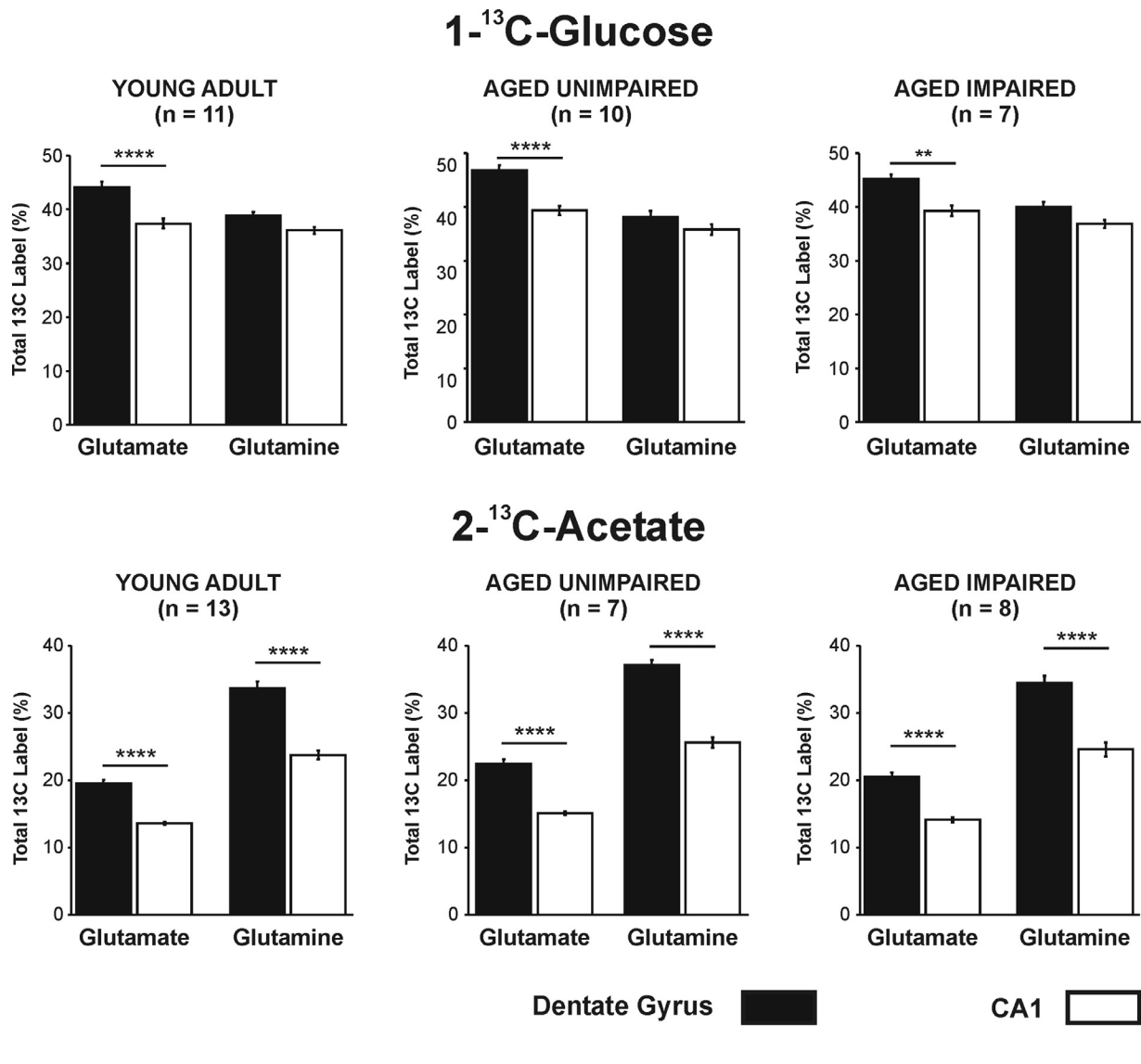
1-^{13}C-Glucose

2-^{13}C-Acetate

Fig. 2. Inter-regional (DG versus CA1) comparison of metabolic incorporation of 1-^{13}C-glucose and 2-^{13}C-acetate into total-labeled glutamate and glutamine. In the presence of ^{13}C glucose (top graphs), note that the percent of total incorporation of ^{13}C label into glutamate was greater in the dentate gyrus in all three behaviorally characterized groups suggesting that the DG may be more metabolically demanding than CA1 (** $p < 0.01$ for AI; **** $p < 0.0001$ for YA and AU). When 2-^{13}C-acetate was added as a metabolic substrate a greater incorporation of label was seen in total glutamine and glutamate in the dentate gyrus versus CA1 in all behaviorally characterized groups ($p \leq 0.0001$ for all comparisons). Further, note that total labeled glutamine levels were greater than that of glutamate reflecting the preferential uptake of acetate into astrocytes. Data are shown as mean ± standard error of the mean.

greater in the dentate gyrus than in CA1 in each of the behaviorally characterized groups (Fig. 2 bottom; $p < 0.0001$ for all comparisons). This result supports the prior suggestion that metabolic activity under resting state conditions in vitro may be greater in the dentate gyrus than CA1. As shown in Fig. 4, significant inter-group differences were also noted for total glutamate labeling in both the dentate gyrus ($F_{2,25} = 5.6$, $p = 0.01$) and area CA1 ($F_{2,25} = 7.6$, $p < 0.005$) subsequent to incubation with 1 mM ^{13}C acetate. Post hoc analysis revealed that total ^{13}C-labeled glutamate was significantly enhanced in AU versus YA rats in both the dentate gyrus and CA1 ($p < 0.01$ in both regions), while YA versus AI and AU versus AI comparisons did not reach significance. The increase in glutamate labeling in AU versus YA rats was also noted when single (M1) ^{13}C-labeled glutamate levels were assessed (Fig. 4, $p < 0.05$ for dentate gyrus; $p < 0.001$ for CA1), although no significant inter-group differences were noted for double (M2) ^{13}C-labeled glutamate. Moreover, while no significant differences were observed in total or sin-
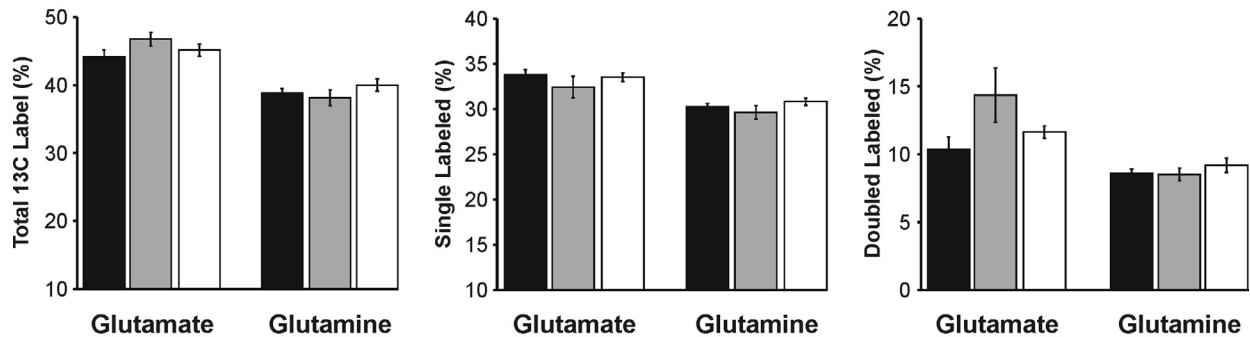
gle ^{13}C-labeled glutamine between the behaviorally characterized groups in either the dentate gyrus or CA1, an increase in double ^{13}C labeled glutamine was detected in AU versus YA and AI samples in the dentate gyrus ($p < 0.05$). This likely reflects increased astrocytic TCA cycle activity metabolizing 2-^{13}C-acetate.

4. Discussion

Reduced glucose utilization has been noted in the hippocampus and cerebral cortex with age and has been correlated with a decline in cognitive function. Our understanding of the consequences and mechanisms involved with these aging-related changes in neural metabolism are unclear due to the ubiquitous utilization of glucose by neurons and astrocytes and the shuttling of metabolic substrates and glutamate/glutamine between these cells. Since data suggest that the neuronal capacity to transport and utilize glucose is decreased with age (e.g., Fattoretti et. al., 2001, 2002; Patel and

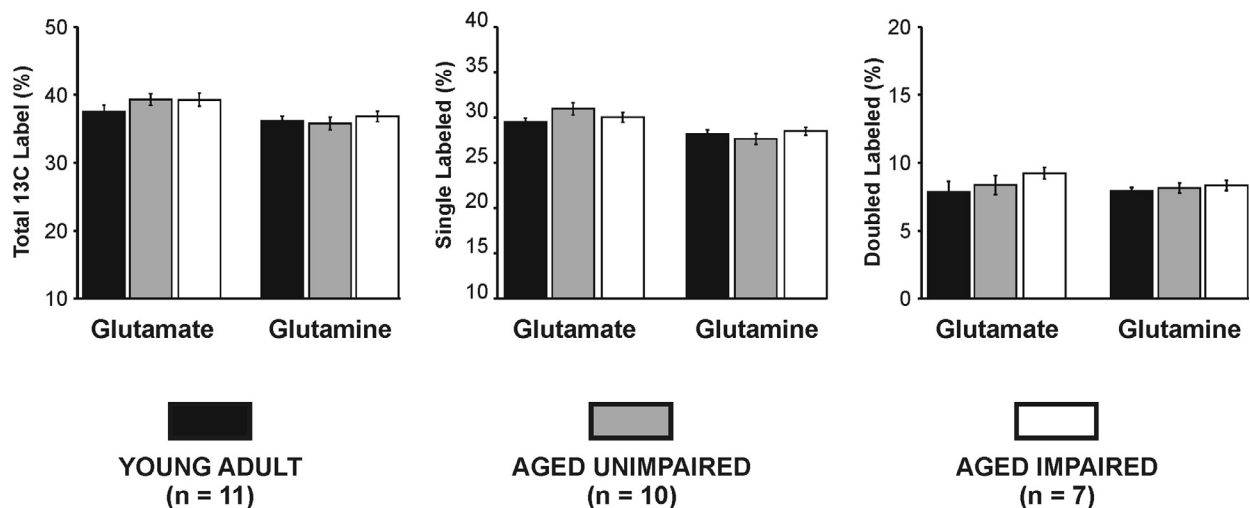# 1-^{13}C-Glucose

A. Dentate Gyrus

B. CA1

Fig. 3. Metabolic incorporation of 1-^{13}C-glucose into glutamate and glutamine in the dentate gyrus and CA1 of YA, AU and AI rats. In each panel, the graph on the left exhibits the total percent label incorporation, the center graph reflects single-label incorporation and the graph on the right shows double-label incorporation. Note that the vertical axes for the graphs depicting total and single-labeling incorporation are truncated (start at 10%) to better illustrate the levels obtained. No significant differences were observed between the behaviorally characterized groups in the percentage of total, single, or double label incorporation into glutamate or glutamine in either the dentate gyrus or CA1. Data are shown as mean ± standard error of the mean.

Brewer, 2003; Boumezbeur et al, 2010) and NMR studies suggest that astroglial TCA cycle activity is increased in humans undergoing successful aging (Boumezbeur et al., 2010), our study examined whether there were differential effects of aging on neuronal and astrocytic metabolism under resting state conditions related to cognitive function using a hippocampal slice model.

The main findings from our study were: (1) the dentate gyrus is metabolically more active than CA1 in vitro, since the percent enrichment of ^{13}C-labeled glutamate and glutamine was consistently higher in the dentate when either glucose or acetate was used as the labeled metabolic substrate; (2) the incorporation of ^{13}C into glutamate and glutamine did not differ between groups when slices from YA, AU and AI rats were incubated in aCSF containing 10 mM 1-^{13}C-glucose; (3) a preferential increase in ^{13}C incorporation in total and single-labeled glutamate was observed in both the dentate gyrus and CA1 of slices from AU rats when 1 mM 2-^{13}C-acetate was added to aCSF containing 10 mM glucose; and 4) the dentate gyrus, but not CA1, of AU rats also exhibited an increased enrichment of ^{13}C double labeled glutamine compared
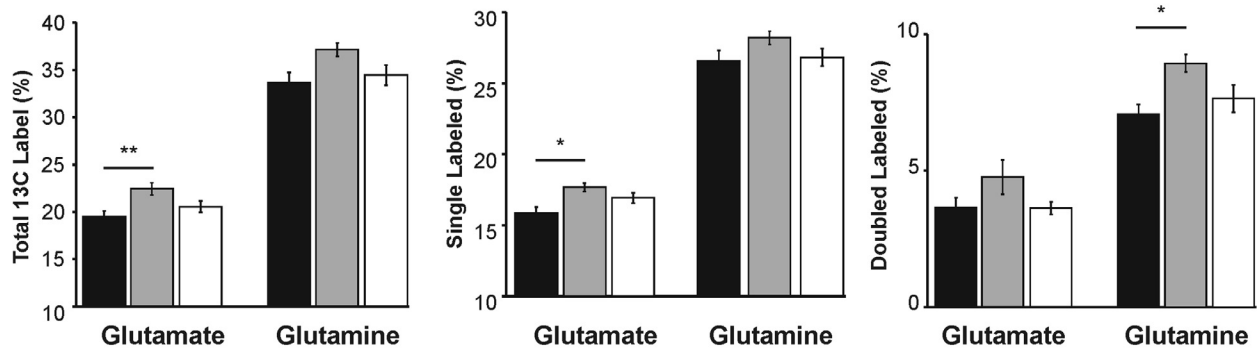
to YA and AI rats. Taken together, these data support the suggestion that astroglial metabolism is selectively enhanced with age in a sub-population of subjects with preserved hippocampal learning and memory.

4.1. 13^C Metabolic substrate incorporation is greater in the dentate gyrus than CA1

Regardless of the metabolic substrate used (1-^{13}C-glucose or 2-^{13}C-acetate), ^{13}C labeling of both glutamate and glutamine was greater in the dentate gyrus than hippocampal region CA1. These results suggest that, in vitro, the dentate gyrus appears to have a greater metabolic activity than CA1 under resting state conditions. This finding is consistent with an 18F-FDG PET study in healthy human volunteers (Cho et al., 2010). However, prior data from rats suggested that CA1 was more metabolically active than the dentate gyrus when 2-DG was infused into behaviorally tested unanesthetized animals (Gage et al., 1984). The reason for the latter discrepancy with our results is unclear, but could reflect differences

2-^{13}C-Acetate

A. Dentate Gyrus

B. CA1

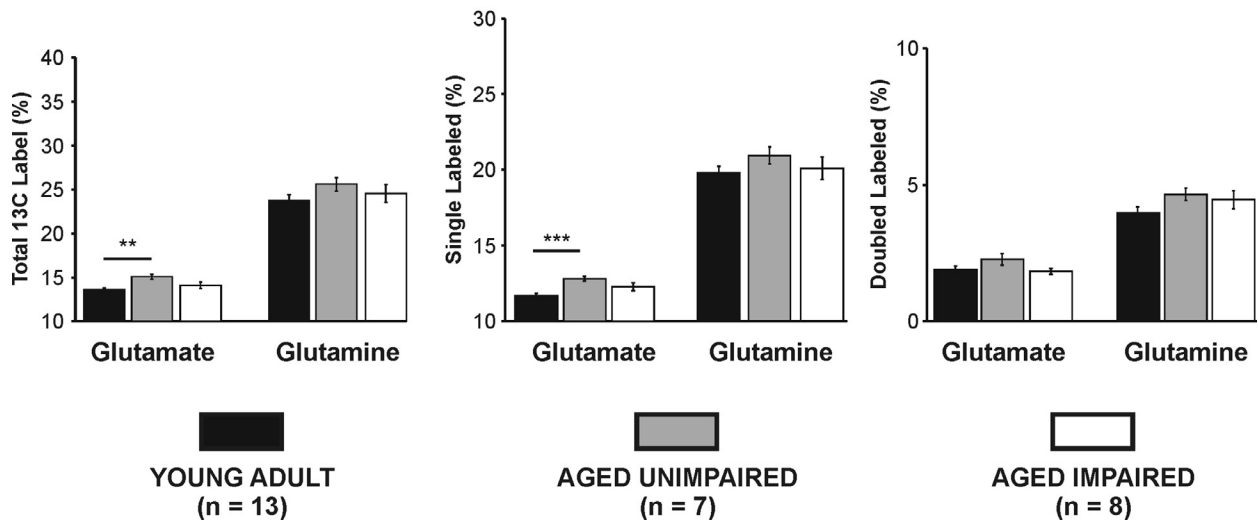| YOUNG ADULT (n = 13) | AGED UNIMPAIRED (n = 7) | AGED IMPAIRED (n = 8) |

Fig. 4. Metabolic incorporation of 2-^{13}C-acetate into glutamate and glutamine in the dentate gyrus and CA1 of YA, AU and AI rats. In each panel, the graph on the left exhibits the total percent label incorporation, the center graph reflects single-label incorporation and the graph on the right shows double-label incorporation. Note that the vertical axes for the graphs depicting total and single-labeling incorporation are truncated (start at 10%) to better illustrate the levels obtained. When ^{13}C acetate was used, a difference in the percent of label incorporation into glutamate and glutamine was observed in the behaviorally characterized groups. Specifically, 1) the percentage of total and single-labeled glutamate was significantly greater in both the dentate gyrus and CA1 of AU rats compared to YA rats, and 2) double- labeled glutamine was increased in the DG of AU rats relative to YA rats. *$p < 0.05$, **$p < 0.01$, ***$p < 0.001$. Data are shown as mean ± standard error of the mean.

in the labelled substrate used or glucose availability or uptake in the in vitro versus in vivo preparations. In addition, our samples of the dentate area included the hilus; it is not clear in Gage et al. whether their analysis was restricted to the dentate granule cell layer.

4.2. 1-^{13}C-glucose and 2-^{13}C-acetate incorporation in slices from YA rats is similar to in vivo results

A time course study in YA rats was performed to assess how the incorporation of ^{13}C-label into glutamate and glutamine in vitro compares with that in vivo. These experiments demonstrated stable slice viability in the in vitro incubation chambers since glucose uptake continued for up to 6 hours and the data suggest there were multiple turns of the TCA cycle as double labeling levels increased with time. A greater percent of glutamate enrichment than that of glutamine was seen when ^{13}C glucose was the labeled substrate, consistent with in vivo studies (e.g., Rothman et al., 2003). While the MS technique presently used did not differentiate which carbon is labeled in singly labeled glutamate or glutamine, NMR data suggest that 1-^{13}C- glucose enters the TCA cycle in neurons via pyruvate dehydrogenase (PDH) and that the expected order of labeling is initially C4 > C3 ≥ C2 > C1, although at isotopic steady state (and in the absence of constant dilutional flows) it is C4 = C3 = C2 = C1; C5 of glutamate and glutamine is not labeled (Moreno et al., 2001; Rothman et al., 2003). Thus, at a very minimum one can interpret that the initial single-labeled glutamate observed in vitro (M1, presumably at C4) is the product of the first turn of the neuronal TCA cy-

cle, with pyruvate entering into alpha-ketoglutarate/glutamate exchange, and that single-labeled glutamine is the result of astrocytic uptake and metabolism of singly-labeled glutamate as well as the metabolism of ^{13}C glucose via the TCA cycle in astrocytes. In contrast, when 2-^{13}C-acetate was used as the metabolic substrate, a greater percent enrichment of total and single labeled glutamine was observed relative to that of glutamate. This result is also consistent with in vivo data and reflects the preferential astrocytic metabolism of acetate (Rothman et al., 2003; Deelchand et al., 2009b). The singly labeled glutamine (i.e., precursor) is then transferred to neurons where it is converted to glutamate via phosphate activated glutaminase (Kvamme et al., 2001; Patel et al., 2010). Interestingly, unlike for ^{13}C-glucose, ^{13}C-acetate incorporation curves do not appear to be as greatly affected by infusion rate (Deelchand et al, 2009a) or anesthesia (Serres et al, 2008) in vivo, suggesting that astroglial metabolism of 2-^{13}C-acetate is saturable and not as strongly linked to neuronal activity as glucose metabolism is (i.e., Sibson et al, 1998).

In general, the current in vitro labeling profiles for single-labeled glutamate and glutamine were remarkably similar to in vivo results, although the rate of incorporation appeared slower (see Serress et al., 2008; Sibson et al. 1998, Patel et al. 2010; Novotny et al, 2001). Possible reasons for this difference include a lack of functional sensory innervation and vascularization in vitro, diffusion constraints placed on the penetration of metabolic substrates into the hippocampal slices (400 µm thick), and lower overall network activity (discussed further below).

4.3. 2-^{13}C-acetate, but not 1-^{13}C-glucose, metabolism in hippocampal slices differentiates AU from AI rats

Data suggest that aging-related CNS hypometabolism correlates with cognitive decline and that numerous aging-related changes are likely to be involved (see Introduction). A surprising finding of the current in vitro experiments was that no significant difference was noted under resting state conditions in the percent enrichment of total and single labeled glutamate or glutamine in either the dentate gyrus or CA1 of AI rats, relative to AU and YA rats when aCSF containing 10 mM 1-^{13}C-glucose was used. As noted above, in vivo data suggest that hippocampal hypometabolism correlates with cognitive decline (e.g., Gage et al., 1984; Mosconi et al., 2008; Croteau et al., 2018; Roy et al., 2014; Riederer et al., 2018). While the reason for this apparent discrepancy with our results is unclear, several factors are likely to be involved. First, any potential aging-related changes in the blood brain barrier (Farrall and Wardlaw, 2009; Stamatovic et al., 2019; Erdo and Krajcsi, 2019) such as altered Glut1 levels (Simpson et al., 1994; Lee et al., 2018; Vogelsang et al., 2018), or a decrease in vascularization (Sonntag et al., 1997; Brown and Thore et al., 2011; Kalaria and Hase, 2019) would not be an issue in vitro. Second, the aging-related decrease in the primary neuronal glucose transporter Glut3 (Fattoretti et al., 2001, 2002) is also unlikely to be an issue since data suggest that the substrate affinity of facilitative glucose transporters (Glut1 and Glut3) is around 1-2 mM (Gorovits and Charron, 2003), much lower than the 10 mM concentration used in our studies. Third, glucose oxidation, and the subsequent incorporation of carbon into glutamate and glutamine, are very closely coupled to brain activity (Sibson et al, 1998; Bader-Goffer et al., 1992; Seress et al., 2008). In vitro slices presumably exhibit lower levels of spontaneous or evoked network activity compared to that in vivo (Novotny et al., 2001). Indeed, in contrast to the in vivo situation where neurotransmitter/neuromodulator systems (e.g., cholinergic system) are known to ramp-up glutamatergic and GABAergic neuronal communication, network oscillations and synchronized activity, biochemical or pharmacological

manipulations are required to induce/amplify such activity in vitro (e.g., Konopacki et al., 1987; Patrylo et al., 1994; Fisahn et al., 1998; Lévesque et al., 2017; Rutecki et al., 1985). Imaging studies that have suggested aging-related cerebral hypometabolism are performed in unanesthetized or only slight anesthetized subjects (Serress et al., 2008; Jagust et al., 2010; Stanley and Raz 2018; Herholtz et al., 2002), and the in vivo experiments of Gage and colleagues (Gage et al., 1984) were done in awake rodents that were only transiently anesthetized with halothane during 2-DG infusion. Additional experiments are required to directly assess whether age-related changes in glucose utilization, relative to altered GLU/GLN cycling and cognitive compromise, can be detected in vitro by challenging slices from behaviorally characterized rats with conditions known to stimulate neural activity, limit glucose availability, or both.

The most interesting finding in the current experiments was the preferential increase in percent enrichment of total and single ^{13}C-labeled glutamate under resting state conditions in the dentate gyrus and CA1 of hippocampal slices from AU rats when 2-^{13}C-acetate was used. These experiments also revealed that the percent enrichment of double-labeled glutamine was increased in the dentate gyrus, but not CA1, in slices from AU rats, compared to those from AI and YA rats. This labeling profile is consistent with enhanced GLU-GLN cycling in the hippocampus of aged rats with cognitive preservation. Specifically, an increase in the shuttling of single labeled glutamine from astrocytes to neurons could result in an increase in total and single labeled glutamate, while the increase in double labeled glutamine could arise from an increase in astrocytic TCA cycle activity. It is unclear whether glutamine synthetase levels or activity change with normal and pathological aging (e.g., Olabarria et al., 2011; Soontornniyomkij et al., 2016; Danh et al., 1985; Bellaver et al., 2017), but existing data suggest that the levels and/or variants of glial excitatory amino acid transporters, EAAT1 and EAAT2, appear to be decreased (Poiter et al, 2010; Schallier et al., 2011; Takahashi et al., 2015; Scott et al., 2011; but see Bellaver et al., 2017). Such a decrease in EAATs would theoretically limit GLU/GLN cycling. However, a study by Boumezbeur et al. (2010) revealed that healthy brain aging was characterized by a decrease in neuron TCA cycle (~28%) activity and a concurrent increase in astroglial TCA cycle (~30%) activity. Taken together with the present results, it is reasonable to conclude that an increase in astroglial TCA cycling may contribute to cognitive preservation during senescence.

This finding is important since it offers some insight into why/how astrocytes may metabolically adapt with age in only a subset of subjects. With advancing age, glucose transport into the brain may decrease (Mooradian et al., 1991) restricting neural glucose uptake and TCA cycle capacity. This could trigger an aging-related shift in astrocytic oxidative metabolism away from glucose to alternate available substrates (e.g., acetate), potentially via pyruvate dehydrogenase phosphorylation (Bogónez et al., 1992; Holness and Sugden, 2003), and result in more glucose being available for neurons. This could be a neuroprotective strategy with subsequent functional preservation up to a limit. As to why this astrocytic adaptation occurs only in a subset of subjects, it has long been known that astrocytes can become reactive in the hippocampus of aged rats (Landfield et al, 1977). Reactive astrocytes exhibit a marked increase in glial fibrillary acidic protein (GFAP). Sugaya and colleagues (Sugaya et al., 1996) have reported an increase in GFAP mRNA expression, but not protein, in the hippocampus of aged rats with impaired hippocampal learning and memory. (Note that VanGuilder et al., 2011 also did not see a differential increase in GFAP protein in a different strain of aged cognitively impaired rats.) Interestingly, administering a sub-therapeutic

dose of ladostigil, a neuroprotective agent, for over six months to 16-month-old rats decreased the aging-related astroglial activation and reduced deficits in spatial learning and memory (Weinstock et al, 2011). In this regard, it should be noted that brain slice preparation has been suggested to induce a shift in astrocytic phenotype into the early stages of reactive gliosis (Takano et al., 2014). We believe that this is unlikely to affect the overall interpretation of the current results however, since identical techniques were used to produce hippocampal slices from all three groups (YA, AU and AI) in the current study and our in vitro data closely reflect the in vivo findings from Boumezbeur et al. (2010) in humans. Thus, although additional experiments are required, it is plausible that hippocampal astrocytes in aged cognitively unimpaired rats do not become reactive and adapt metabolically to utilize alternative available substrates, thereby helping preserve neuronal function and cognition.

While the current set of experiments did not directly assess peripheral metabolism (e.g., fasting glucose/ketone levels, glucose tolerance, insulin-sensitivity) it is interesting to note that previous studies have shown an association between changes in peripheral metabolism and age as well as cognitive performance (Macklin et al., 2017; Griffith et al., 2019; reviewed in Frazier et al., 2019). Thus, future studies will be performed to directly examine this potential interaction between peripheral and CNS metabolism. Additionally, it is also interesting to consider whether the preservation of glutamate labeling in aCSF containing 10 mM ^{13}C-labeled glucose under resting conditions could, in part, reflect the astrocytes converting labeled glucose into labeled lactate for neuronal utilization as has been proposed by Pellerin and Magistretti (2012) and has been suggested to occur in vivo activated conditions (Sampol et al., 2013). Additional experiments using NMR are required however, to directly assess this mechanism by following the position of the labeled carbon over time.

5. Conclusions

In summary, two metabolic substrates (1-^{13}C-glucose and 2-^{13}C-acetate) were used in this study to assess ^{13}C-incorporation into glutamate and glutamine under resting state conditions in the dentate gyrus and CA1 with respect to age and cognitive function. The ^{13}C-glucose data obtained suggest that the association reported between cognitive decline and altered glucose uptake/utilization in vivo may arise due to metabolic challenge (e.g., such as occurs during the performance of a cognitive task) and were not evaluated in our in vitro studies. Further, the findings with 2-^{13}C-acetate indicate that astroglial metabolism and subsequently GLU-GLN cycling may be enhanced in the dentate gyrus and CA1 in a compensatory manner that helps preserve hippocampal cognitive function. Thus, aging-related cognitive preservation may entail an astrocytic metabolic shift to compensate for altered neuronal metabolism. Therapies targeting astrocytes to reduce their activation and/or boost their metabolic activity and/or GLU/GLN cycling may aid in reversing/limiting age-related cognitive decline.

Disclosure statement

The authors do not have any conflict of interest to report.

Acknowledgments

Supplementary materials

Supplementary material associated with this article can be found, in the online version, at doi:10.1016/j.neurobiolaging.2021.02.015.

References

Badar-Goffer, R, Bachelard, H, Morris, P, 1990. Cerebral metabolism of acetate and glucose studied by 13C-n.m.r. spectroscopy. Biochem. J. 266, 133–139.

Bellaver, B, Souza, DG, Souza, DO, Quincozes-Santos, A., 2017. Hippocampal astrocyte cultures from adult and aged rats reproduce changes in glial functionality observed in the aging brain. Mol. Neurobiol. 54 (4), 2969–2985.

Bogónez, E, Gómez-Puertas, P, Satrústegui, J., 1992. 1992 Pyruvate dehydrogenase dephosphorylation in rat brain synaptosomes and mitochondria: evidence for calcium-mediated effect in response to depolarization, and variations due to ageing. Neurosci. Lett. 142, 123–127.

Boumezbeur, F, Mason, G, Graaf, R, Behar, K, Cline, G, Shulman, G, Rothman, D, Petersen, K., 2010. Altered brain mitochondrial metabolism in healthy aging as assessed by in vivo magnetic resonance spectroscopy. J. Cereb. Blood Flow Metab. 30, 211–221.

Brown, WR, Thore, CR., 2011. Review: cerebral microvascular pathology in ageing and neurodegeneration. Neuropathol. Appl. Neurobiol. 37 (1), 56–74.

Chaudry, F, Schmitz, D, Reimer, R, Larsson, P, Gray, A, Nicoll, R, Kavanaugh, M, Edwards, R., 2002. Glutamine uptake by neurons: interaction of protons with system A transporters. J. Neurosci. 22, 62–72.

Cho, ZH, Son, YD, Kim, HK, Kim, ST, Lee, SY, Chi, JG, Park, CW, Kim, YB., 2010. Substructural hippocampal glucose metabolism observed on PET/MRI. J. Nucl. Med. 51 (10), 1545–1548.

Crimins, JL, Pooler, A, Polydoro, M, Luebke, JI, Spires-Jones, TL., 2013. The intersection of amyloid ß and tau in glutamatergic synaptic dysfunction and collapse in Alzheimer's disease. Ageing Res. Rev. 12 (3), 757–763.

Croteau, E, Castellano, CA, Fortier, M, Bocti, C, Fulop, T, Paquet, N, Cunnane, SC., 2018. A cross-sectional comparison of brain glucose and ketone metabolism in cognitively healthy older adults, mild cognitive impairment and early Alzheimer's disease. Exp. Gerontol. 107, 18–26.

d'Avila, JC, Siqueira, LD, Mazeraud, A, Azevedo, EP, Foguel, D, Castro-Faria-Neto, HC, Sharshar, T, Chrétien, F, Bozza, FA., 2018. Age-related cognitive impairment is associated with long-term neuroinflammation and oxidative stress in a mouse model of episodic systemic inflammation. J. Neuroinflamm. 15 (1), 28.

Danh, H, Benedetti, S, Dostert, P., 1985. Age-related changes in glutamine synthetase activity of rat brain, liver, and heart. Gerontology 31, 95–100.

Daulatzai, MA., 2017. Cerebral hypoperfusion and glucose hypometabolism: key pathophysiological modulators promote neurodegeneration, cognitive impairment, and Alzheimer's disease. J. Neurosci. Res. 95 (4), 943–972.

Deelchand, D, Nelson, C, Shestov, A, Ugurbil, K, Henry, P, 2009a. Simultaneous measurement of neuronal and glial metabolism in rat brain in vivo using co-infusions of [1,6-^{13}C2] glucose and [1,2-^{13}C$_2$] acetate. J. Magn. Reason 196, 157–163.

Dericioglu, N, Garganta, CL, Petroff, OA, Mendelsohn, D, Williamson, A., 2008. Blockade of GABA synthesis only affects neural excitability under activated conditions in rat hippocampal slices. Neurochem. Int. 53 (1-2), 22–32.

Disterhoft, JF, Thompson, LT, Moyer, JR, Mogul, DJ., 1996. Calcium-dependent after-hyperpolarization and learning in young and aging hippocampus. Life Sci. 59, 413–420.

Dröge, W, Schipper, HM., 2007. Oxidative stress and aberrant signaling in aging and cognitive decline. Aging Cell 6 (3), 361–370.

Erdő, F, Krajcsi, P., 2019. Age-related functional and expressional changes in efflux pathways at the blood-brain barrier. Front. Aging Neurosci 11, 196.

Escartin, C, Valette, V, Lebon, V, Bonvento, G., 2006. Neuron-astrocyte interactions in the regulation of brain energy metabolism: a focus on NMR spectroscopy. J. Neurochem. 99, 393–401.

Farrall, AJ, Wardlaw, JM., 2009. Blood-brain barrier: ageing and microvascular disease—systematic review and meta-analysis. Neurobiol. Aging 30 (3), 337–352.

Fattoretti, P, Bertoni-Freddari, C, Casoli, T, Di Stefano, G, Solazzi, M, Giorgetti, B., 2001. Decreased expression of glucose transport protein (Glut3) in aging and vitamin E deficiency. Ann. N. Y. Acad. Sci. 973, 293–296.

Fattoretti, P, Bertoni-Freddari, C, Di Stefano, G, Casoli, T, Gracciotti, N, Solazzi, M, Pompei, P., 2002. Quantitative immunohistochemistry of glucose transport protein (Glut3) expression in the rat hippocampus during aging. J. Histochem. Cytochem. 49, 671–672.

Fayed, N, Andrés, E, Viguera, L, Modrego, PJ, Garcia-Campayo, J., 2014. Higher glutamate+glutamine and reduction of N-acetylaspartate in posterior cingulate according to age range in patients with cognitive impairment and/or pain. Acad. Radiol. 21 (9), 1211–1217.

Fisahn, A, Pike, FG, Buhl, EH, Paulsen, O., 1998. Cholinergic induction of network oscillations at 40 Hz in the hippocampus in vitro. Nature 394 (6689), 186–189.

Frazier, HN, Ghoweri, AO, Anderson, KL, Lin, RL, Porter, NM, Thibault, O., 2019. Broadening the definition of brain insulin resistance in aging and Alzheimer's disease. Exp. Neurol. 313, 79–87.

Gage, F, Kelly, P, Björklund, A, 1984. 1984 Regional changes in brain glucose metabolism reflect cognitive impairments in aged rats. J. Neurosci. 4, 2856–2865.

Gorovits, N, Charron, M., 2003. What we know about facilitative glucose transporters. Biochem. Mol. Biol. Educ. 31, 163–172.

Ghosh, D, LeVault, KR, Barnett, AJ, Brewer, GJ., 2012. A reversible early oxidized redox state that precedes macromolecular ROS damage in aging nontransgenic and 3xTg-AD mouse neurons. J. Neurosci. 32 (17), 5821–5832.

Griffith, CM, Macklin, LN, Cai, Y, Sharp, AA, Yan, XX, Reagan, LP, Strader, AD, Rose, GM, Patrylo, PR., 2019. Impaired glucose tolerance and reduced plasma insulin precede decreased AKT phosphorylation and GLUT3 translocation in the hippocampus of old 3xTg-AD mice. J. Alzheimers Dis. 68 (2), 809–837.

Herholz, K, Salmon, E, Perani, D, Baron, JC, Holthoff, V, Frölich, L, Schönknecht, P, Ito, K, Mielke, R, Kalbe, E, Zündorf, G, Delbeuck, X, Pelati, O, Anchisi, D, Fazio, F, Kerrouche, N, Desgranges, B, Eustache, F, Beuthien-Baumann, B, Menzel, C, Schröder, J, Kato, T, Arahata, Y, Henze, M, Heiss, WD., 2002. Discrimination between Alzheimer dementia and controls by automated analysis of multicenter FDG PET. Neuroimage 17 (1), 302–316.

Hertz, L, Peng, L, Dienel, GA, 2007. Energy metabolism in astrocytes: high rate of oxidative metabolism and spatiotemporal dependence on glycolysis/glycogenolysis. J. Cereb. Blood Flow Metab. 27 (2), 219–249.

Holness, M, Sugden, M., 2003. Regulation of pyruvate dehydrogenase complex activity by reversible phosphorylation. Biochem. Soc. Trans. 31, 1963–2003.

Huang, D, Liu, D, Yin, J, Qian, T, Shrestha, S, Ni, H., 2017. Glutamate-glutamine and GABA in brain of normal aged and patients with cognitive impairment. Eur. Radiol. 27 (7), 2698–2705.

Jagust, WJ, Bandy, D, Chen, K, Foster, NL, Landau, SM, Mathis, CA, Price, JC, Reiman, EM, Skovronsky, D, Koeppe, RA., 2010. Alzheimer's disease neuroimaging initiative. The Alzheimer's disease neuroimaging initiative positron emission tomography core. Alzheimers Dement 6 (3), 221–229.

Jenstad, M, Quazi, AZ, Zilberter, M, Haglerød, C, Berghuis, P, Saddique, N, Goiny, M, Buntup, D, Davanger, S, S Haug, FM, Barnes, CA, McNaughton, BL, Ottersen, OP, Storm-Mathisen, J, Harkany, T, Chaudhry, FA, 2009. System A transporter SAT2 mediates replenishment of dendritic glutamate pools controlling retrograde signaling by glutamate. Cereb. Cortex 19 (5), 1092–1106.

Kalaria, RN, Hase, Y, 2019. Neurovascular ageing and age-related diseases. Subcell. Biochem. 91, 477–499.

Konopacki, J, MacIver, MB, Bland, BH, Roth, SH, 1987. Carbachol-induced EEG 'theta' activity in hippocampal brain slices. Brain Res. 405 (1), 196–198.

Kumar, A, Foster, TC., 2019. Alteration in NMDA receptor mediated glutamatergic neurotransmission in the hippocampus during senescence. Neurochem. Res. 44 (1), 38–48.

Kvamme, E, Torgner, I, Roberg, B., 2001. Kinetics and localization of brain phosphate activate glutaminase. J. Neurosci. Res. 66, 951–958.

Landfield, P, Lynch, G., 1977. Impaired monosynaptic potentiation in in vitro hippocampal slices from aged, memory-deficient rats. J. Gerontol. 5, 523–533.

Landfield, P, Rose, G, Sandles, L, Wohlstadter, T, Lynch, G., 1977. Patterns of astroglial hypertrophy and neuronal degeneration in the hippocampus of aged, memory deficient rats. J. Gerontol. 32, 3–12.

Lee, KY, Yoo, DY, Jung, HY, Baek, L, Lee, H, Kwon, HJ, Chung, JY, Kang, SH, Kim, DW, Hwang, IK, Choi, JH., 2018. Decrease in glucose transporter 1 levels and translocation of glucose transporter 3 in the dentate gyrus of C57BL/6 mice and gerbils with aging. Lab. Anim. Res. 34 (2), 58–64.

Lennie, P., 2003. The cost of cortical computation. Curr. Biol. 13 (6), 493–497.

Lévesque, M, Cataldi, M, Chen, LY, Hamidi, S, Avoli, M., 2017. Carbachol-induced network oscillations in an in vitro limbic system brain slice. Neurosci 21 (348), 153–164.

Liu, J, Head, E, Gharib, AM, Yuan, W, Ingersoll, RT, Hagen, TM, Cotman, CW, Ames, BN., 2002. Memory loss in old rats is associated with brain mitochondrial decay and RNA/DNA oxidation: partial reversal by feeding acetyl-L-carnitine and/or R-alpha -lipoic acid. Proc. Natl Acad. Sci. 99, 2356–2361.

Macklin, L, Griffith, CM, Cai, Y, Rose, GM, Yan, XX, Patrylo, PR., 2017. Glucose tolerance and insulin sensitivity are impaired in APP/PS1 transgenic mice prior to amyloid plaque pathogenesis and cognitive decline. Exp. Gerontol. 88, 9–18.

Manyevitch, R, Protas, M, Scarpiello, S, Deliso, M, Bass, B, Nanajian, A, Chang, M, Thompson, SM, Khoury, N, Gonnella, R, Trotz, M, Moore, DB, Harms, E, Perry, G, Clunes, L, Ortiz, A, Friedrich, JO, Murray, IV., 2018. Evaluation of metabolic and synaptic dysfunction hypotheses of Alzheimer's disease (AD): a meta-analysis of CSF markers. Curr. Alzheimer Res. 15 (2), 164–181.

Martinez-Hernandez, A, Bell, KP, Norenberg, MD., 1977. Glutamine synthetase: glial localization in brain. Science 195 (4284), 1356–1358.

McNay, E, Gold, P., 2001. Age-related differences in hippocampal extracellular fluid concentration during behavioral testing and following systemic glucose administration. J. Gerontol. 56A B66-B71.

Moreno, A, Blüml, S, Hwang, JH, Ross, BD., 2001. Alternative 1-^{13}C-glucose infusion protocols for clinical ^{13}C MRS examinations of the brain. Magn. Reson. Med. 46 (1), 39–48.

Motsinger-Reif, AA, Zhu, H, Kling, MA, Matson, W, Sharma, S, Fiehn, O, Reif, DM, Appleby, DH, Doraiswamy, PM, Trojanowski, JQ, Kaddurah-Daouk, R, SE, Arnold, 2013. Comparing metabolomic and pathologic biomarkers alone and in combination for discriminating Alzheimer's disease from normal cognitive aging. Acta. Neuropathol. Commun. 1, 28.

Mooradian, A, Morin, A, Cipp, L, Haspel, H., 1991. Glucose transport is reduced in the blood-brain barrier of aged rats. Brain Res. 551, 145–149.

Morley, JE, Farr, SA, 2014. The role of amyloid-beta in the regulation of memory. Biochem. Pharmacol. 88 (4), 479–485.

Mosconi, L, De Santi, S, Li, J, Tsui, W, Li, Y, Boppanna, M, Laska, E, Rusinek, H, de Leon, M., 2008. Hippocampal hypometabolism predicts cognitive decline from normal aging. Neurobiol. Aging 29, 676–692.

Navarro, A, López-Cepero, J, Bández, M, Sánchez-Pino, M, Gómez, C, Cadenas, E, Boveris, A., 2008. Hippocampal mitochondrial dysfunction in rat aging. Am. J. Physiol. 294 R501-R509.

Navakkode, S, Liu, C, Soong, TW., 2018. Altered function of neuronal L-type calcium channels in ageing and neuroinflammation: implications in age-related synaptic dysfunction and cognitive decline. Ageing Res. Rev. 42, 86–99.

Nilsen, LH, Melø, TM, Saether, O, Witter, MP, Sonnewald, U., 2012. Altered neurochemical profile in the McGill-R-Thy1-APP rat model of Alzheimer's disease: a longitudinal in vivo ^{1}H MRS study. J. Neurochem. 123 (4), 532–541.

Novotny Jr, EJ, Ariyan, C, Mason, GF, O'Reilly, J, Haddad, GG, Behar, KL., 2001. Differential increase in cerebral cortical glucose oxidative metabolism during rat postnatal development is greater in vivo than in vitro. Brain Res. 888 (2), 193–202.

Oh, MM, Oliveira, FA, Waters, J, Disterhoft, JF., 2013. Altered calcium metabolism in aging CA1 hippocampal pyramidal neurons. J. Neurosci. 33 (18), 7905–7911.

Olabarria, M, Noristani, HN, Verkhratsky, A, Rodríguez, JJ., 2011. Age-dependent decrease in glutamine synthetase expression in the hippocampal astroglia of the triple transgenic Alzheimer's disease mouse model: mechanism for deficient glutamatergic transmission? Mol. Neurodegener. 6, 55.

Patel, J, Brewer, G, 2003. Age-related changes in neuronal glucose uptake in response to glutamate and ß-amyloid. J. Neurosci. Res. 72, 527–536.

Patel, A, Graaf, R, Rothman, D, Behar, K, Mason, G., 2010. Evaluation of cerebral acetate metabolic rates in rat brain in vivo using ^{1}H[^{13}C]-NMR. J. Cereb. Blood Flow Metab. 30, 1200–1213.

Patrylo, PR, Schweitzer, JS, Dudek, FE., 1994. Potassium-dependent prolonged field bursts in the dentate gyrus: effects of extracellular calcium and amino acid receptor antagonists. Neuroscience 61 (1), 13–19.

Patrylo, PR, Williamson, A., 2007. The effects of aging on dentate circuitry and function. Prog. Brain Res. 163, 679–696.

Pereda, D, Al-Osta, I, Okorocha, AE, Easton, A, Hartell, NA., 2019. Changes in presynaptic calcium signaling accompany age-related deficits in hippocampal LTP and cognitive impairment. Aging Cell. 18 (5) e13008.

Pellerin, L, Magistretti, PJ., 2012. Sweet sixteen for. ANLS 32 (7), 1152–1166.

Potier, B, Billard, JM, Rivière, S, Sinet, PM, Denis, I, Champeil-Potokar, G, Grintal, B, Jouvenceau, A, Kollen, M, Dutar, P., 2010. Reduction in glutamate uptake is associated with extrasynaptic NMDA and metabotropic glutamate receptor activation at the hippocampal CA1 synapse of aged rats. Aging Cell 9 (5), 722–735.

Raskin, J, Cummings, J, Hardy, J, Schuh, K, Dean, RA., 2015. Neurobiology of Alzheimer's disease: integrated molecular, physiological, anatomical, biomarker, and cognitive aspects. Curr. Alzheimer Res. 12 (8), 712–722.

Riederer, I, Bohn, KP, Preibisch, C, Wiedemann, E, Zimmer, C, Alexopoulos, P, Förster, S., 2018. Alzheimer disease and mild cognitive impairment: Integrated pulsed arterial spin-labeling MRI and ^{18}F-FDG PET. Radiology 288 (1), 198–206.

Riese, F, Gietl, A, Zölch, N, Henning, A, O'Gorman, R, Kälin, AM, Leh, SE, Buck, A, Warnock, G, Edden, RA, Luechinger, R, Hock, C, Kollias, S, Michels, L., 2015. Posterior cingulate γ-aminobutyric acid and glutamate/glutamine are reduced in amnestic mild cognitive impairment and are unrelated to amyloid deposition and apolipoprotein E genotype. Neurobiol. Aging 36 (1), 53–59.

Rosenzweig, ES, Barnes, CA., 2003. Impact of aging on hippocampal function: plasticity, network dynamics, and cognition. Prog. Neurobiol. 69 (3), 143–179.

Rothman, DL, Behar, KL, Hyder, F, Shulman, RG., 2003. In vivo NMR studies of the glutamate neurotransmitter flux and neuroenergetics: implications for brain function. Annu. Rev. Physiol. 65, 401–427.

Rothman, DL, De Feyter, HM, de Graaf, RA, Mason, GF, Behar, KL., 2011. 13C MRS studies of neuroenergetics and neurotransmitter cycling in humans. NMR Biomed. 24 (8), 943–957.

Rothman, D, Sibson, N, Hyder, F, Shen, J, Behar, K, Shulman, R, 1999. In vivo nuclear magnetic resonance spectroscopy studies of the relationship between the glutamate-glutamine neurotransmitter cycle and functional neuroenergetics. Philos Trans. R. Soc. Lond. 354, 1165–1177.

Rothstein, JD, Dykes-Hoberg, M, Pardo, CA, Bristol, LA, Jin, L, Kuncl, RW, Kanai, Y, Hediger, MA, Wang, Y, Schielke, JP, Welty, DF, 1996. Knockout of glutamate transporters reveals a major role for astroglial transport in excitotoxicity and clearance of glutamate. Neuron 16 (3), 675–686.

Rowe, W, Blalock, E, Chen, K, Kadish, I, Wang, D, Barrett, J, Thibault, O, Porter, N, Rose, G, Landfield, P., 2007. Hippocampal expression analyses reveal selective associated of immediate-early, neuroenergetic, and myelinogenic pathways with cognitive impairment in aged rats. J. Neurosci. 27, 3098–3110.

Roy, K, Pepin, LC, Philiossaint, M, Lorius, N, Becker, JA, Locascio, JJ, Rentz, DM, Sperling, RA, Johnson, KA, Marshall, GA., 2014. Regional fluorodeoxyglucose metabolism and instrumental activities of daily living across the Alzheimer's disease spectrum. J. Alzheimers Dis. 42 (1), 291–300.

Rutecki, PA, Lebeda, FJ, Johnston, D., 1985. Epileptiform activity induced by changes in extracellular potassium in hippocampus. J. Neurophysiol. 54 (5), 1363–1374.

Sampol, D, Ostrofet, E, Jobin, M-L, Raffard, G, Sanchez, S, Bouchaud, V, Franconi, J-M, Bonvento, G, 2013. Bouzier-Sore A-K. Glucose and lactate metabolism in the awake and stimulated rat: a (13)C-NMR study. Front. Neuroenerget. 5 (5), 1–11.

Schallier, A, Smolders, I, Van Dam, D, Loyens, E, De Deyn, PP, Michotte, A, Michotte, Y, Massie, A., 2011. Region- and age-specific changes in glutamate trans-

port in the AßPP23 mouse model for Alzheimer's disease. J. Alzheimers Dis. 24 (2), 287–300.

Scott, HA, Gebhardt, FM, Mitrovic, AD, Vandenberg, RJ, Dodd, PR., 2011. Glutamate transporter variants reduce glutamate uptake in Alzheimer's disease. Neurobiol. Aging 32 (3), 553 e1-11.

Serres, S, Raffard, G, Franconi, J, Merle, M, 2008. Close coupling between astrocytic and neuronal metabolisms to fulfill anaplerotic and energy needs in the rat brain. J. Cereb. Blood Flow Metab. 28, 712–724.

Sibson, N, Dhankhar, A, Mason, G, Rothman, D, Behar, K, Shulman, R., 1998. Stoichiometric coupling of brain glucose metabolism and glutamatergic neuronal activity. PNAS Proc. Natl. Acad. Sci. 95, 316–321.

Simpson, IA, Chundu, KR, Davies-Hill, T, Honer, WG, Davies, P., 1994. Decreased concentrations of GLUT1 and GLUT3 glucose transporters in the brains of patients with Alzheimer's disease. Ann. Neurol. 35 (5), 546–551.

Sonntag, WE, Lynch, CD, Cooney, PT, Hutchins, PM., 1997. Decreases in cerebral microvasculature with age are associated with the decline in growth hormone and insulin-like growth factor 1. Endocrinol 138 (8), 3515–3520.

Soontornniyomkij, V, Kesby, JP, Soontornniyomkij, B, Kim, JJ, Kisseleva, T, Achim, CL, Semenova, S, Jeste, DV., 2016. Age and high-fat diet effects on glutamine synthetase immunoreactivity in liver and hippocampus and recognition memory in mice. Curr. Aging Sci. 9 (4), 301–309.

Stamatovic, SM, Martinez-Revollar, G, Hu, A, Choi, J, Keep, RF, Andjelkovic, AV., 2019. Decline in sirtuin-1 expression and activity plays a critical role in blood-brain barrier permeability in aging. Neurobiol. Dis. 126, 105–116.

Stanley, JA, Raz, N., 2018. Functional magnetic resonance spectroscopy: the "new" MRS for cognitive neuroscience and psychiatry research. Front. Psychiatry 9, 76.

Sugaya, K, Chouinard, M, Greene, R, Robbins, M, Personett, D, Kent, C, Gallagher, M, McKinney, M, 1996. Molecular indices of neuronal and glial plasticity in the hippocampal formation in rodent model of age-induced spatial learning impairment. J. Neurosci. 16 (10), 3427–3443.

Takahashi, K, Kong, Q, Lin, Y, Stouffer, N, Schulte, DA, Lai, L, Liu, Q, Chang, LC, Dominguez, S, Xing, X, Cuny, GD, Hodgetts, KJ, Glicksman, MA, Lin, CL., 2015. Restored glial glutamate transporter EAAT2 function as a potential therapeutic approach for Alzheimer's disease. J. Exp. Med. 212 (3), 319–332.

Takano, T, He, W, Han, X, Wang, F, Xu, Q, Wang, X, Oberheim Bush, NA, Cruz, N, Dienel, GA, Nedergaard, M, 2014. Rapid manifestation of reactive astrogliosis in acute hippocampal brain slices. Glia 62 (1), 78–95.

Tardif, CL, Devenyi, GA, Amaral, RSC, Pelleieux, S, Poirier, J, Rosa-Neto, P, Breitner, J, Chakravarty, MMPREVENT-AD Research Group, 2018. Regionally specific changes in the hippocampal circuitry accompany progression of cerebrospinal fluid biomarkers in preclinical Alzheimer's disease. Hum. Brain Mapp. 39 (2), 971–984.

Thibault, O, Landfield, PW., 1996. Increase in single L-type calcium channels in hippocampal neurons during aging. Science 272, 1017–1020.

Toescu, EC, Verkhratsky, A., 2007. The importance of being subtle: small changes in calcium homeostasis control cognitive decline in normal aging. Aging Cell 6 (3), 267–273.

Tombaugh, GC, Rowe, WB, Chow, AR, Michael, TH, Rose, GM., 2002. Theta-frequency synaptic potentiation in CA1 in vitro distinguishes cognitively impaired from unimpaired aged Fischer 344 rats. J. Neurosci. 22 (22), 9932–9940.

Tu, S, Okamoto, S, Lipton, SA, Xu, H., 2014. Oligomeric $A\beta$-induced synaptic dysfunction in Alzheimer's disease. Mol. Neurodegener. 9, 48.

VanGuilder, HD, Bixler, GV, Brucklacher, RM, Farley, JA, Yan, H, Warrington, JP, Sonntag, WE, Freeman, WM., 2011. Concurrent hippocampal induction of MHC II pathway components and glial activation with advanced aging is not correlated with cognitive impairment. J. Neuroinflamm. 8, 138.

Vogelsang, P, Giil, LM, Lund, A, Vedeler, CA, Parkar, AP, Nordrehaug, JE, Kristoffersen, EK., 2018. Reduced glucose transporter-1 in brain derived circulating endothelial cells in mild Alzheimer's disease patients. Brain Res. 1678, 304–309.

Waagepetersen, HS, Sonnewald, U, Larsson, OM, Schousboe, A., 2000. Compartmentation of TCA cycle metabolism in cultured neocortical neurons revealed by ^{13}C MR spectroscopy. Neurochem. Int. 36 (4-5), 349–358.

Weinstock, M, Luques, L, Poltyrev, T, Bejar, C, Shoham, S., 2011. Ladostigil prevents age-related glial activation and spatial memory deficits in rats. Neurobiol. Aging 32, 1069–1078.

Wyss, MT, Magistretti, PJ, Buck, A, Weber, B., 2011. Labeled acetate as a marker of astrocytic metabolism. J. Cereb. Blood Flow Metab. 31, 1668–1674.